

ELASTIC PLASTIC NON-CONFORMING CONTACT MODELING PART II: RESULTS AND DISCUSSIONS

FRUNZA Gheorghe, SPINU Sergiu

University "Stefan cel Mare" of Suceava, ROMANIA
ghfrunza@gmail.com, sergiu.spinu@fim.usv.ro

Keywords: numerical simulation, elastic-plastic contact, hardening law, residual state.

Abstract: The contact between a rigid sphere and an elastic-plastic half-space is modeled using the newly proposed computer program. The elastic-plastic behavior is described by a power hardening law (Swift). Numerical predictions agree well with results obtained from alternative numerical codes or from finite element analysis. The plastic strain region, initially hemispherical, advances peripherally toward the free surface, enveloping a purely elastic core on the central axis. Numerical simulations predict that residual stresses decrease the peak intensity of the stresses induced by contact pressure, thus impeding further plastic flow. Computed pressure distributions appear flattened compared to elastic case, due to changes in both hardening state and contact conformity.

1. INTRODUCTION

An efficient algorithm for elastic - plastic contact modeling is proposed in a companion paper. Implementation of three-dimensional spectral methods in evaluation of residual state contribution and of Fotiu and Nemat-Nasser's universal algorithm for integration of elastoplasticity equations, [4], is expected to decrease dramatically the computational requirements, thus allowing for finer grids in the numerical simulation.

In this paper, numerical predictions of the newly proposed algorithm are compared with already published results, thus validating the computer code. Development of plastic strains and of residual stresses with application of new loading increments is assessed, and contribution of residual state, which superimpose elastic state induced by contact pressure, is suggested.

Algorithm refinements allow for a fine grid, of $120 \times 120 \times 80$ cells, to be imposed in the computational domain. A good agreement with existing results is found, giving confidence in the newly advanced program.

2. ELASTIC-PLASTIC CONTACT PARAMETERS

The contact between a rigid sphere of radius $R = 105 \cdot 10^{-6} m$ and an elastic-plastic half-space is modeled, allowing for comparison with results published by Boucly, Nélias and Green, [2]. Elastic half-space parameters are: Young modulus, $E_2 = 210 GPa$, Poisson's ratio, $\nu_2 = 0,3$. The hardening law of the elastic-plastic material is chosen as a power law (Swift), according to El Ghazal, [3]:

$$\sigma_Y(e^p) = B(C + e^p)^n, \quad (1)$$

with $\sigma_Y(e^p)$ the yield strength function, e^p the effective accumulated plastic strain, expressed in microdeformations, and the following parameters: $B = 1280 MPa$, $C = 30$, $n = 0.085$. The imposed hardening curve is depicted in Fig. 1.

The contact is loaded incrementally to a maximum value of $W = 0.650 N$, for which the purely elastic model predicts a contact radius $a_H = 6.053 \mu m$ and a hertzian pressure $p_H = 8470 MPa$.

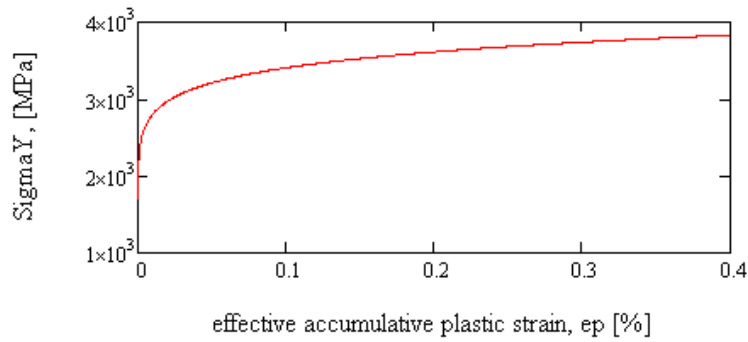


Figure 1. Swift's hardening law

Dimensionless coordinates are defined as ratios to a_H , $\bar{x}_i = x_i/a_H$, and dimensionless pressure or stresses as ratios to p_H . The computational domain is a rectangular cuboid of sides $L_1 = L_2 = 3a_H$, $L_3 = 1.6a_H$, which is discretized with the following parameters: $N_1 = N_2 = 120$, $N_3 = 80$ parameters. Due to the fact that problem is axisymmetric, three dimensional distributions are depicted in the plane $x_2 = 0$ only.

Pressure profiles predicted by the numerical program for six loading levels corresponding to elastic-plastic domain are depicted in Fig. 2. Hertz pressure corresponding to maximum load is also plotted for reference.

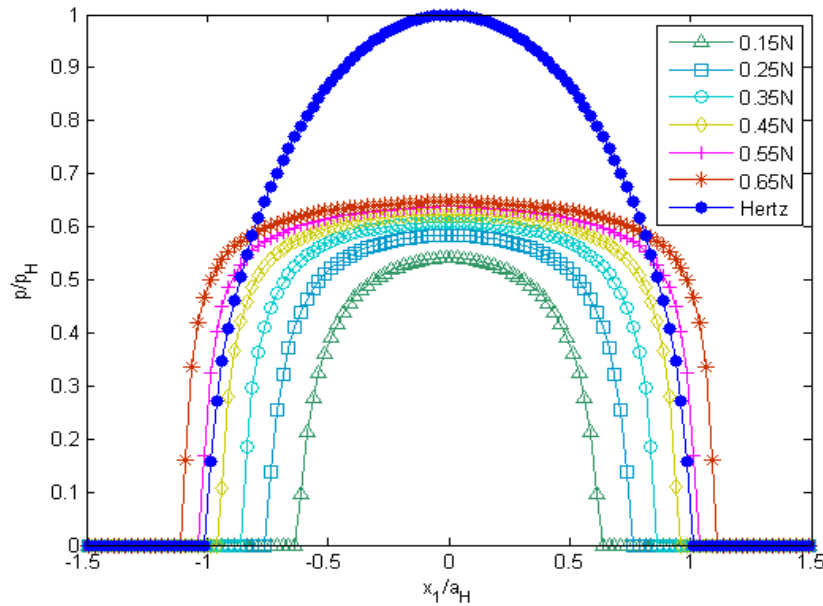


Figure 2. Pressure profiles in the plane $x_2 = 0$, various loading levels

Elastic-plastic pressure distributions appear flattened compared to the purely elastic case. At the end of the loading loop, a central plateau of uniform pressure can be observed in the vicinity of $6.5p_H$. This limitation of contact pressure results in an increased elastic-plastic contact radius, compared to elastic counterpart a_H .

The same behavior is predicted by Jacq. et al. [5], by Boucly, Nélias and Green, [2], using load driven (ld) or displacement driven (dd) formulations, Fig. 3, and also by Benchea and Cretu, [1], using finite element analysis, Fig. 4.

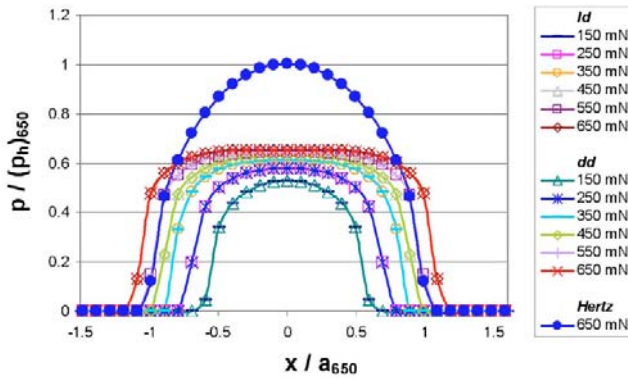


Figure 3. Pressure profiles obtained by numerical simulation, [2]

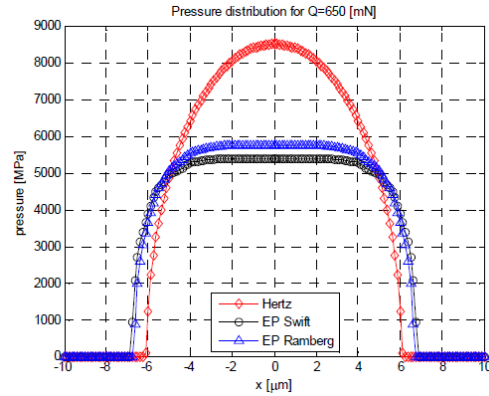


Figure 4. Pressure profiles obtained by finite element analysis, [1]

4. DEVELOPMENT OF RESIDUAL STATE

Initiation of plastic flow occurs on the central axis of the contact, in the point where von Mises equivalent stress exceeds initial yield strength. With application of new loading increments, plastic strain region expands, occupying a hemispherical domain, Fig. 5.

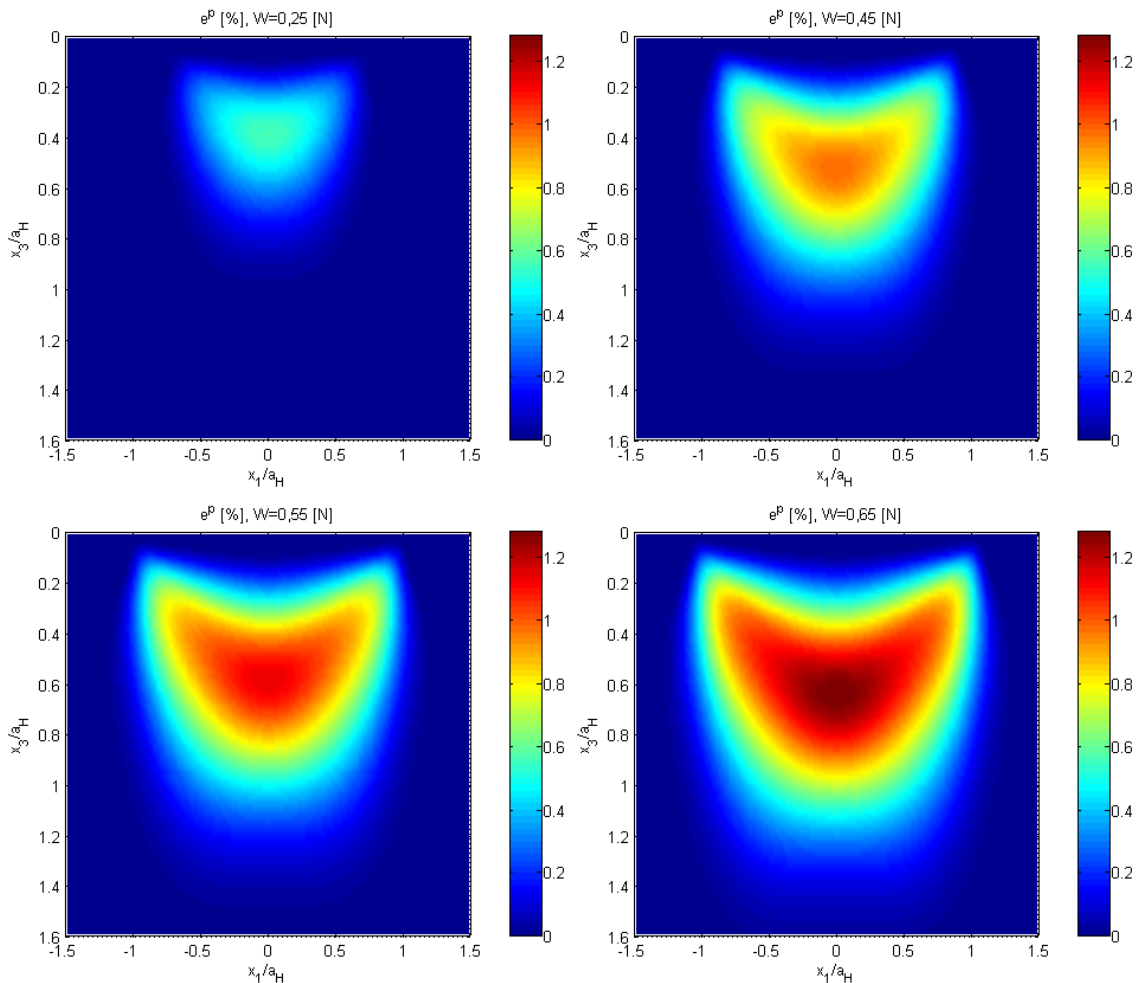


Figure 5. Development of effective accumulated plastic strain with loading level

In this domain, corresponding to elastic-plastic range, elastic and plastic strains are of the same order of magnitude. Toward the end of the loading cycle, the plastic core approach peripherally the free surface, enveloping a purely elastic central region. In this range, corresponding to a fully plastic state, displaced material shifts toward indenter sides. This development is consistent with the one presented by Wang and Keer, [7].

Plastic strain region induces residual stresses which modify the stresses generated by contact pressure. Intensity of residual stresses is not negligible, as shown in the following section. At the end of the loading cycle, residual stress tensor components follow the distributions depicted in Fig. 6.

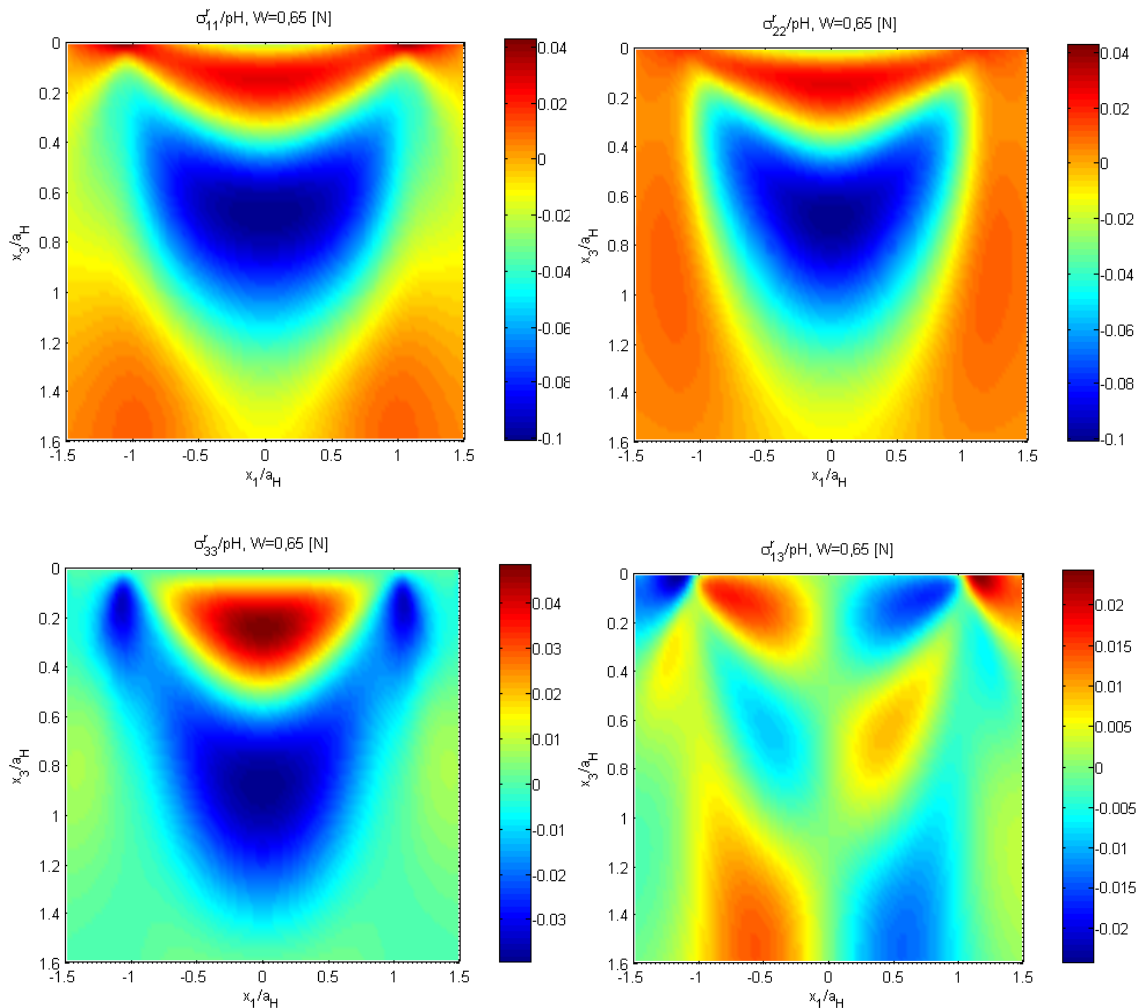


Figure 6. Residual stress tensor components at the end of the loading cycle

3. RESIDUAL STATE CONTRIBUTION

Plastic strain region generates residual displacements, namely displacements that would persist if a purely elastic unloading would occur. As shown in [6], this displacements increase contact conformity, resulting in a more uniform pressure distribution on an enlarged contact area.

Plastic strains also induce residual stresses, namely elastic stresses which would persist after unloading. These residual stresses superimpose stresses induced by contact pressure, the resulting state being responsible for further plastic strain. Consequently, an accurate estimation of stress field in the elastic-plastic body is essential to plastic strain

increment prediction. According to theory of plasticity, yielding only occurs when the stress point reaches the current yield locus, and a further plastic flow can be enforced only by increasing the stress to a point outside the yield locus. In its turn, the yield locus evolves to enclose the new stress point.

Figures 7 and 8 depict distributions of equivalent von Mises residual and contact stress. Summation of these two states yields elastic-plastic stress state, presented in Fig. 9. Residual stress intensity is one order of magnitude smaller than equivalent contact stress. Comparison of distributions depicted in figures 8 and 9 suggests that residual stress reduces peaks in contact stress intensity, thus making the resulting field more uniform. This behavior is also suggested by the curves traced in Fig. 10. Maximum intensity of contact stress increase more rapidly than the maximum of the total field, due to contribution of residual stress. Consequently, residual stresses act to impede further plastic yielding.

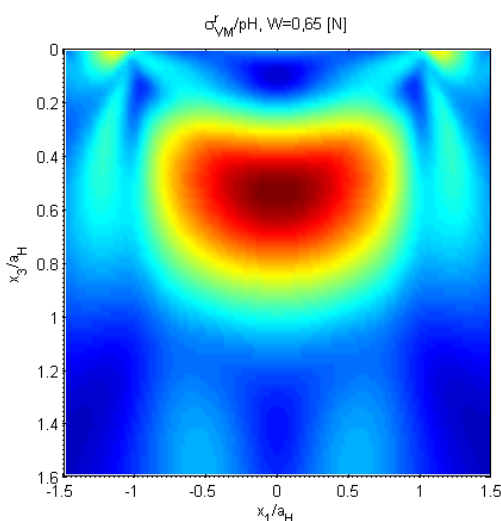


Figure 7. Von Mises residual stress

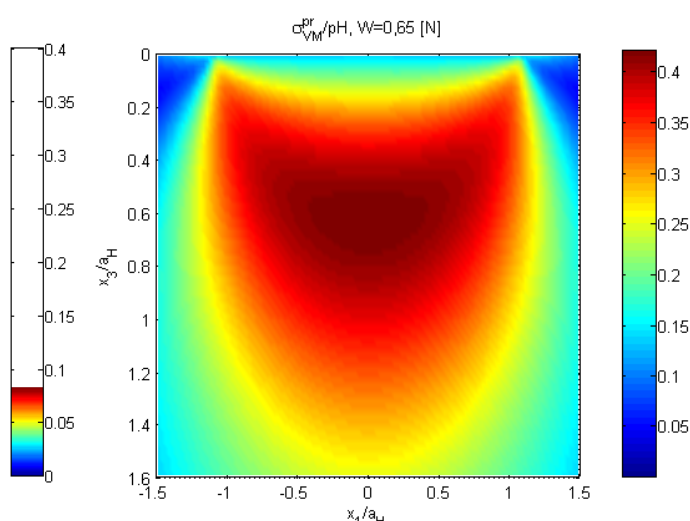


Figure 8. Von Mises contact stress

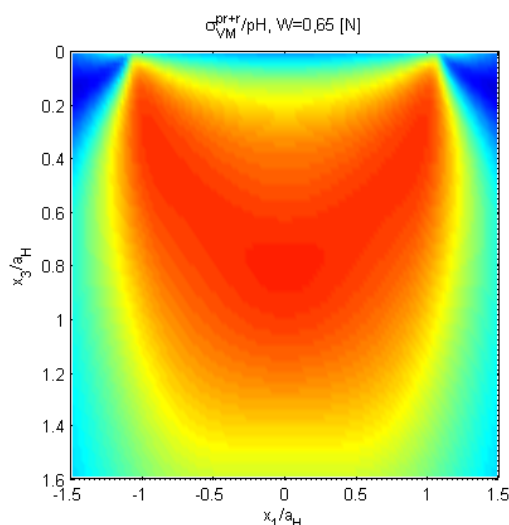


Figure 9. Resulting Von Mises stress in elastic-plastic body

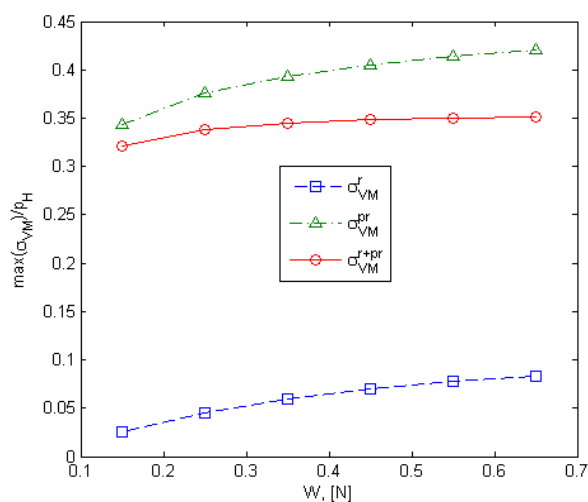


Figure 10. Maximum intensities of stress fields versus loading level

On the central axis of the contact, residual and contact stress tensor components vary according to figures 11 and 12. The normal residual stress σ_{33}^r is nil on the free surface, tensile immediately under the surface and compressive at hertzian depths. On the other hand, normal contact stress σ_{33}^{pr} is compressive.

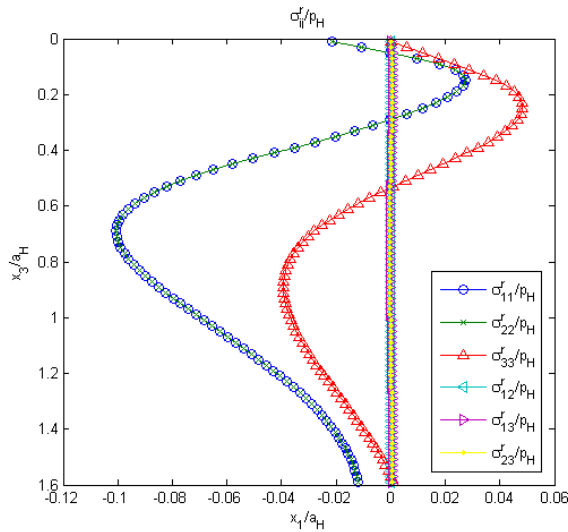


Figure 11. Residual stress tensor components on the central axis of the contact

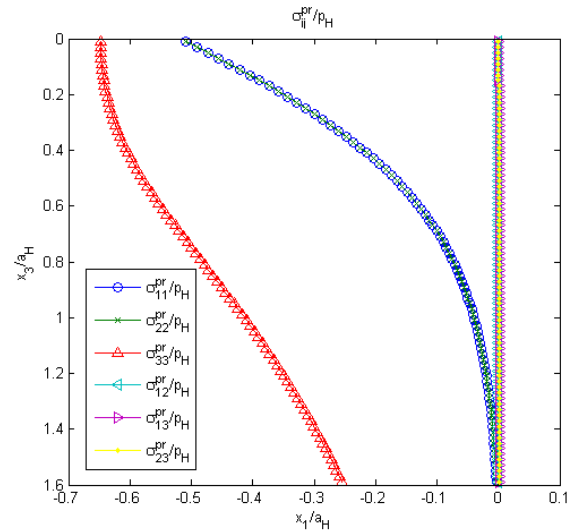


Figure 12. Contact stress tensor components on the central axis of the contact

The residual hydrostatic pressure, defined as $\sigma_h^r = I_1^r / 3$, where I_1^r is the first invariant of residual stress tensor, is compressive immediately under the surface and at hertzian depths, and tensile in between. Its maximum is located at a greater depth than the one for the hydrostatic pressure (induced by contact pressure), as depicted in figures 13 and 14.

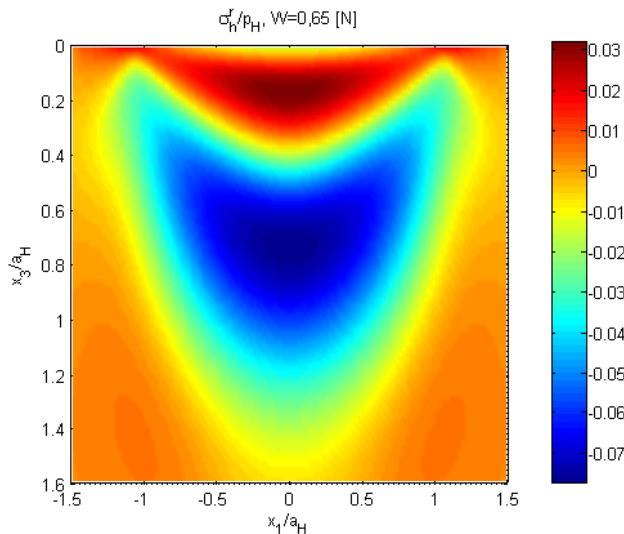


Figure 13. Residual hydrostatic pressure in the plane $x_2 = 0$

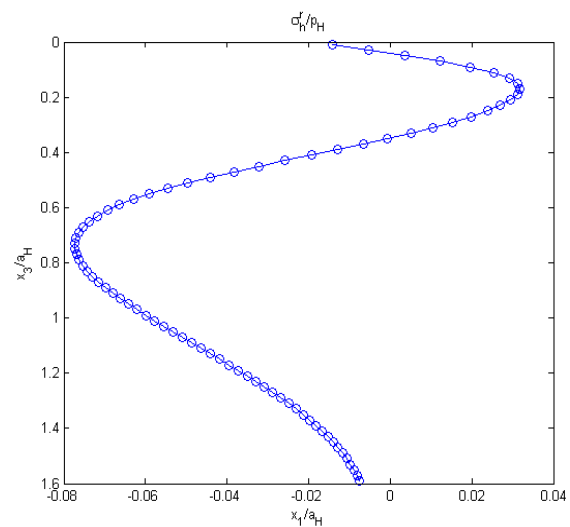


Figure 14. Residual hydrostatic pressure on the central axis of the contact

4. CONCLUSIONS

The newly proposed elastic-plastic contact program is used to model the contact between a rigid sphere and an elastic-plastic half-space following a Swift isotropic hardening law. Pressure profiles predicted numerically agree well with already published results. Pressure appears flattened compared to the elastic case, due to changes in both hardening state and contact conformity.

Plastic zone, initially occupying a hemispherical region located at hertzian depths, advances toward the free surface with increased loading, enveloping a purely elastic core. This development is consistent with existing models for the elastic-plastic process, marking the passing from elastic-plastic range to fully plastic.

Distributions of residual stress components are also depicted. Residual stress intensity is one order of magnitude smaller than stresses induced by contact pressure. They contribute to the total elastic field by decreasing the peaks in contact pressure intensity, thus impeding further plastic flow. The resulting field is more uniform, suggesting that material responds by change in hardening state as to delay further plastic flow until the stress point touches the new yield locus.

REFERENCES

- [1] Benchea, M, and Crețu, S., (2008), *An Improved Incremental Model to Analyse Elastic - Plastic Concentrated Contacts – The Finite Element Analysis and Validation*, Acta Tribologica, Vol. 16, ISSN 1220-8434.
- [2] Boucly, V., Nélías, D., and Green, I., (2007), *Modeling of the Rolling and Sliding Contact Between Two Asperities*, ASME J. Tribol., 129, pp. 235 - 245.
- [3] El Ghazal, H., (1999), *Etude des propriétés microstructurales et mécaniques des aciers 16NiCrMo13 cémenté et 32CrMoV13 nitrure - Application à la prévision de leur limite d'endurance en fatigue de roulement*, Ph.D. Thesis, INSA Lyon, France.
- [4] Fotiu, P. A., and Nemat-Nasser, S., (1996), *A Universal Integration Algorithm for Rate-Dependant Elastoplasticity*, Comput. Struct., 59, pp. 1173–1184.
- [5] Jacq, C., Nélías, D., Lormand, G., and Girodin, D., (2002), *Development of a Three-Dimensional Semi-Analytical Elastic-Plastic Contact Code*, ASME J. Tribol., 124, pp. 653–667.
- [6] Spinu, S., (2009), *Contributions to the Solution of the Elastic-Plastic Normal Contact Problem*, (in Romanian), PhD Thesis, University of Suceava, Romania.
- [7] Wang, F., and Keer, L. M., (2005), *Numerical Simulation for Three Dimensional Elastic-Plastic Contact With Hardening Behavior*, ASME J. Tribol., 127, pp. 494–502.